JOURNAL OF MATERIALS SCIENCE 26 (1991) 5411–5419

An approach to the mechanical behaviour of SiC/SiC and C/SiC ceramic matrix composites

Part 2 *Theoretical approach*

E. INGHELS,** J. LAMON*
Ecole Nationale Supérieure des Mines de Paris, Centre des Materiaux, BP 87, 91003 EVRY Cedex, France

A model is proposed for the mechanical behaviour of continuous fibre-reinforced ceramics. This model was applied to the bidirectional SiC/SiC and C/SiC composites examined in Part 1 of the present paper. This model satisfactorily predicted the load–displacement relations for bending specimens, from an intrinsic constitutive law based on data measured in tension. However, the results were weakened by the significant scatter exhibited by experimental data. The constitutive law was also theoretically determined from matrix and fibre properties: matrix cracking was predicted by an approach generalizing the Aveston–Cooper–Kelly theory, predictions of fibre failure used numerical simulations. Theoretical values were significantly overestimated, which was attributed to the contribution of microstructural flaws to the fracture process.

1. Introduction

The mechanical behaviour of two SiC matrix composites was investigated in Part 1 of the present paper [1]. These composites consist of a bidirectional woven framework of carbon or SiC fibre bundles impregnated by the SiC matrix. Tensile and bending tests at room temperature have shown that the damaging process could be related to the typical structure of the composites. Two types of damage were observed: multiple matrix cracking prior to fibre failure as usually observed in undirectional composites with a brittle matrix [2, 3], and frictional phenomena within or between the bundles.

The mechanical response of these composites was mainly related to the behaviour of the fibre bundles impregnated with SiC matrix which were considered as entities. The mechanical response was characterized using stress–elastic strain relations measured in the region of fracture. These relations are described by linear two-part curves, which is consistent with the theoretical predictions available for unidirectional composites [3]. The linear limit and ultimate fracture were related to matrix cracking and to fibre failure, respectively. The damage was characterized using residual strain and the amount of energy stored in the specimen. Data showed a continuous increase with elastic strain above a threshold comparable to the linearity limit in the stress–elastic strain relation.

The experimental results suggested that the above-mentioned set of characteristics are appropriate to describe the mechanical behaviour of both composites. But they also revealed certain shortcomings of the analysis. The main limitation of the analysis dealt with the stress–elastic strain curves, which are distinct in tensile and bending conditions. According to previous studies [2, 4], this loading geometry effect may be attributed to simplified calculations. In particular, the composites were assumed to be linear elastic until fracture. The analysis was also unable to separate the respective contributions of the bundles and the framework to composite damage.

The analysis reported in Part 1 [1] was thus completed by developing a theoretical model aimed at predicting the mechanical behaviour of composites from a material intrinsic stress–elastic strain relation.

Prediction of the load–displacement curves used a non-linear constitutive law. This topic has received some emphasis in previous studies [4, 5]; the authors usually introduced a constitutive law in numerical computations of stress and strain distributions. Two kinds of law were proposed. The simpler one has an arbitrary shape (usually a power law similar to that used for metals), with parameters derived from experimental data obtained from tensile tests [5]. However, because these laws have no physical meaning in the case of composites, they cannot be easily related to the damaging process and to fibres and matrix properties. Laws [4] also used a theoretical law based on the damaging process established for a tensile loading geometry. However, extension to other geometries requires certain refinements, and the relation between the theoretical law and the real behaviour of the composite is not straightforward. The effect of specimen geometry is partially hindered by the influence of

Present address: Laboratoire des Composites Thermostructuraux, Europarc, 1–3 Avenue Léonard de Vinci, 33600, Pessac, France.
** SEP, BP 802, 27200 VERNON, FRANCE.

0022–2461/91 $03.00 + .12

the microstructure on the constitutive law. This paper focuses on an intermediate solution. A constitutive law was selected on the basis that it could be related to the damaging process and that the parameters could be measured on tensile tests. The effect of the test fixture compliance on fracture was also taken into account in the load–displacement curve simulation.

Prediction of the ultimate fracture was based on the statistical distribution of strengths for individual fibres. Previous studies devoted to the prediction of fibre failure considered non-brittle matrices [6, 7]. These predictions consist of numerical simulations of the failure process assuming various stress transfers from broken fibres to the neighbouring ones, and different criteria for ultimate fracture. A similar simulation method is proposed in the present paper, considering stress transfers and fracture criteria with regard to matrix brittleness.

The model was applied to both the C/SiC and SiC/SiC composites, and the predicted behaviour was compared with the experimental results. The model was able to predict the differences previously observed between tensile and bending results, and also the part allocated to the bundles in the residual damage.

2. Model for mechanical behaviour of composites

2.1. Definition of the constitutive law

The composites were regarded as unidirectional. Only the damage operating on the bundles parallel to the applied load was considered. The damaging process is described in Fig. 1. It was assumed that:

(i) no damage occurred either in compression, or at applied strains smaller than ε_{a1};

(ii) multiple cracking in the matrix initiated at strain ε_{a1}. The distance l_a between two consecutive cracks was assumed constant,

(iii) beyond ε_{a1}, there was no further matrix damage, until fibre failure at strain ε_{a2}.

The constitutive law was defined as depicted in Fig. 2. This law describes the mechanical response of an elementary cell, representative of the composite, e.g. a fibre of length, l_a, surrounded by matrix. The volume fractions of fibre, V_f, and matrix, V_m, are identical to those prevailing in the composites. This unit cell was suggested by the periodical nature of matrix cracking. The constitutive law thus characterizes an homogeneous material having exactly the same mechanical behaviour as the composite. It was defined

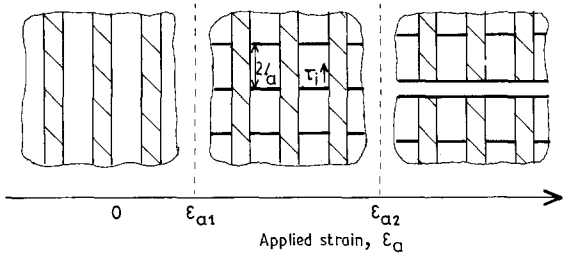

Figure 1 Schematic diagram showing the damaging process considered in the model.

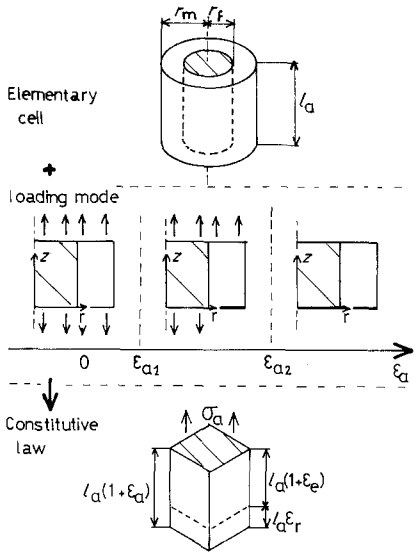

Figure 2 Schematic diagram summarizing the definition of the constitutive law. It characterizes the mechanical behaviour of an elementary cell, and can subsequently be applied to any volume of material, whatever its real structure.

using a set of data which can be measured experimentally or expressed theoretically in terms of fibre and matrix properties. The constitutive law is the keystone of the present model, because

(i) it provides a characteristic of the material, allowing a description of loading geometry effects on the mechanical behaviour (Section 2.2);

(ii) it relates the mechanical behaviour of composite to fibre and matrix properties (Section 2.3).

The constitutive law describes the variations of the applied stress, σ_a, the elastic, ε_e, and residual, ε_r, components of the applied strain, ε_a, and the elastic, W_e, and absorbed, W_f, energies per unit volume, with the applied strain, ε_a. The constitutive law was determined from the following basic equations

$$\varepsilon_a = \frac{1}{l_a}\int \varepsilon_f(z)\,dz \quad (1)$$

$$\sigma_a = E_f V_f \varepsilon_f(z) + E_m V_m \varepsilon_m(z) \quad (2)$$

$$\varepsilon_e = 2\,W_e/\sigma_a \quad (3)$$

$$\varepsilon_r = \varepsilon_a - \varepsilon_e \quad (4)$$

$$W_e = \tfrac{1}{2}\left[E_f \varepsilon_f(z)^2 + E_m \varepsilon_m(z)^2\right] \quad (5)$$

$$W_f = \frac{\gamma_m V_m}{l_a} + \int \frac{2V_f \tau(z)}{r_f l_a} |v_f(z) - v_m(z)|\,dz \quad (6)$$

The symbols are defined in Fig. 2. $\varepsilon_f(z)$ and $\varepsilon_m(z)$ are the strains in the fibre and the matrix, respectively, along the z-axis (the strain components perpendicular to fibre axis were neglected). The absorbed energy, W_f, is the sum of the surface energy and of a frictional term for interfacial fibre shifting. $v_f(z)$ and $v_m(z)$ are the displacements in the fibre and the matrix, respectively.

Prior to matrix cracking, $\varepsilon_f(z)$ and $\varepsilon_m(z)$ are uniform and identical. The constitutive law is thus linear elastic, and the elastic modulus is given by the law of mixture.

In the cracked composites, the shear stress was assumed constant along the interface. Strains are there-

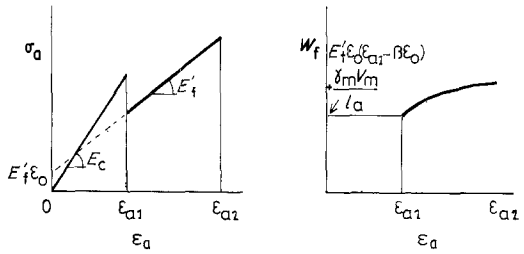

Figure 3 Determination of the constitutive law parameters from plots of applied stress, σ_a, and absorbed energy, W_f, against applied strain, ε_a.

fore given by [3]

$$\varepsilon_f(z) = (\sigma_a - 2\tau_i z)\frac{1}{E_f V_f} \quad (7)$$

$$\varepsilon_m(z) = \frac{2V_f\tau_i}{r_f V_m E_m} z \quad (8)$$

where the symbols are again defined in Fig. 2. The constitutive law is defined by a set of six parameters, E_c, E'_f, ε_0, ε_{a1}, ε_{a2} and $\gamma_m V_m/l_a$, as indicated by Table I. These characteristics can be measured experimentally as shown in Fig. 3. They can also be calculated theoretically by comparing the mechanical behaviour of the composite with fibre and matrix properties, as described in a subsequent section.

2.2. Simulation of load–displacement curves, for tensile and bending geometries

A two-step simulation was carried out. Load–displacement relations were determined using the constitutive law for the typical strain distributions induced on loading within the specimens (the curve is described by increasing values of the applied strain). This gave all the equilibrium positions of the specimen in the load–displacement chart. The effects of test fixture were taken into account in a second step only, by considering energy transfers. This revealed that some parts of the equilibrium curve could not be reached during tests.

TABLE I Equations defining the constitutive law: parameters are stiffness E'_f and E_c, strains ε_0, ε_{a1} and ε_{a2}, energy density $\gamma_m V_m/l_a$.

	$-\infty < \varepsilon_a < \varepsilon_{a1}$	$\varepsilon_{a1} < \varepsilon_a < \varepsilon_{a2}$
σ_a	$E_c\varepsilon_a$	$E'_f(\varepsilon_a + \varepsilon_0)$
ε_a	ε_a	$\dfrac{\varepsilon_a^2 + \beta\varepsilon_0^2}{\varepsilon_a + \varepsilon_0}$
ε_r	0	$\varepsilon_0\dfrac{\varepsilon_a - \beta\varepsilon_0}{\varepsilon_a + \varepsilon_0}$
W_e	$\frac{1}{2}E_c\varepsilon_a$	$\frac{1}{2}E'_f(\varepsilon_a^2 + \beta\varepsilon_0^2)$
W_{fv}	0	$\dfrac{\gamma_m V_m}{l_a} + E'_f\varepsilon_0(\varepsilon_a - \beta\varepsilon_0)$

$$E'_f = E_f V_f \qquad E_c = E_f V_f + E_m V_m \qquad \beta = \frac{E_c + 3E'_f}{3(E_c - E'_f)}$$

$$\varepsilon_0 = \frac{\tau_i l_a}{E_f r_f} \quad \text{and} \quad \varepsilon_0 \leqslant \frac{E_c - E'_f}{E_c + E'_f}\varepsilon_{a1}$$

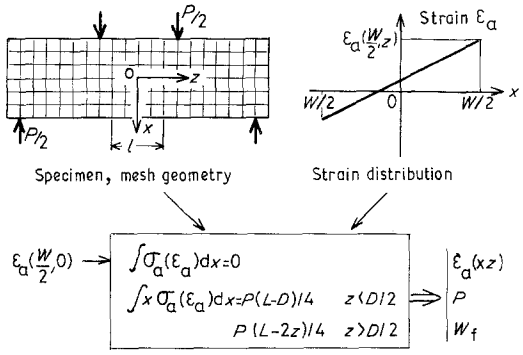

Figure 4 Method for the determination of the load–displacement relations and the equation of absorbed energy, W_f, using equilibrium conditions in bending specimens.

The strain distribution was assumed uniform within tensile specimens. The equilibrium curve was thus easily predicted from the constitutive law. In bending specimens, the strain distribution was assumed to vary linearly along both thickness and longitudinal directions. This usual hypothesis is still valid with the orthotropic materials of the present paper [4]. The strain distribution was determined using the equilibrium conditions in the cross-section as indicated in Fig. 4. It was completely described using the strain at the centre of the outer surface. The displacement, δ, measured on testing was calculated by summing strains along a certain distance, l, on the tensile surface, and the applied load was derived from the momentum in cross-section (Fig. 4).

Evaluation of energy transfers between specimens and the loading environment considered perfectly elastic test fixtures. As described in Fig. 5, the applied load was obtained from the cross-head position, δ_t, using a condition of equilibrium between specimen and fixture. Instability was determined from energy balance considerations for the whole specimen, as shown in Fig. 6. It was assumed that instability induced a decrease in the total energy, and a minimum of elastic energy. This problem was solved by considering the areas under the load–displacement curves. An instability appeared possible at sudden drops in load.

The theoretical load–displacement curves were then analysed using the method developed for the experimental results in Part 1 [1], the material being characterized by a reversible $\sigma(\varepsilon_e)$ and a residual ($\varepsilon_r(\varepsilon_e)$ and $W_f(\varepsilon_e)$) behaviour, where σ is the average applied

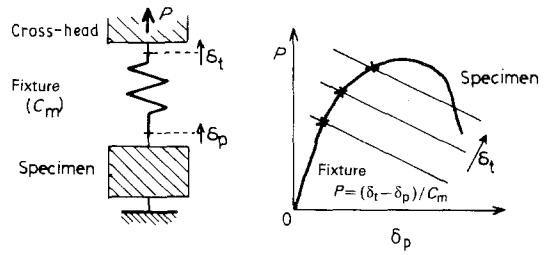

Figure 5 Schematic diagram showing the equilibrium of the system specimen + test fixture (C_m is fixture compliance). In the load–displacement chart (P–δ_p), a test is described by increasing values of the cross-head displacement (δ_t).

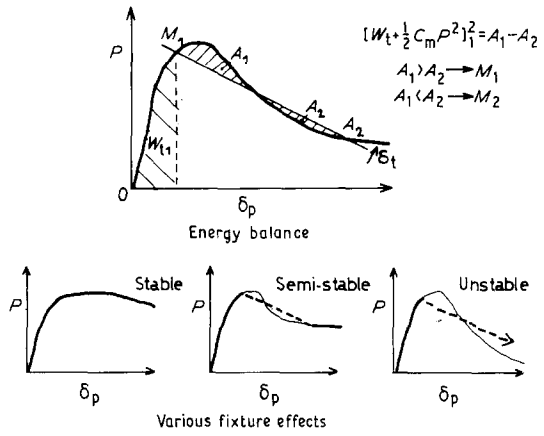

Figure 6 Graphical determination of equilibrium positions, based on an energy balance. Depending on load–displacement curve, elasticity of the test fixture can cause stable, semi-stable or unstable fracture.

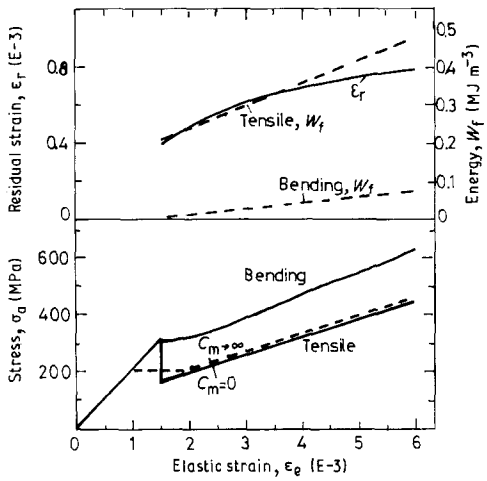

Figure 7 Example of theoretical behaviour for a model composite ($E_f' = 57$ GPa, $E_c = 245$ GPa, $\varepsilon_0 = 0.11\%$, $\varepsilon_{a1} = 0.16\%$, $\gamma_m V_m / l_a = 1.35$ MJ m^{-3}). The reversible behaviour $\sigma_a(\varepsilon_e)$ is shown for tensile and bending loading geometries. For the tensile geometry, the solid and dotted lines correspond to hard and soft fixtures, respectively. The residual behaviour is given by $\varepsilon_r(\varepsilon_e)$ (——) and by $W_f(\varepsilon_e)$ (– – –). Tensile and bending results are characterized by the same $\varepsilon_r(\varepsilon_e)$ plot.

stress. Theoretical plots are shown in Fig. 7 for both specimen geometries. Because there is no drop in load during a bending test, no effect of the fixtures is predicted. In contrast, in the tensile test, the stiffness of the fixture has some influence on matrix cracking. On testing, the test fixture was significantly less stiff than the specimens. The load could thus be considered as constant during matrix cracking. A critical strain, ε_{a1}, lower than in bending tests, is predicted. It is worth noting that this lower value is consistent with the critical strain predicted by the Aveston–Cooper–Kelly (ACK) theory (see Fig. 8).

2.3. Relation between constitutive law and fibre and matrix properties: theoretical constitutive law

Table I suggests that the constitutive law is completely defined by ε_{a1}, ε_{a2} and l_a. The critical strain of the

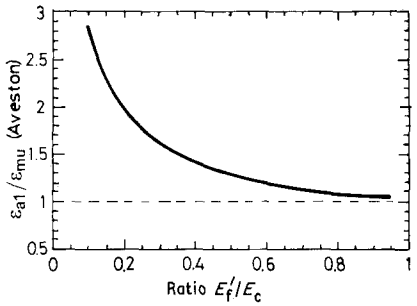

Figure 8 Comparison of the critical strain, ε_{a1}, with the matrix fracture strain predicted by ACK theory, ε_{mu}, for tensile specimens.

matrix, ε_{a1}, and the length, l_a, were calculated using an energy-based method inspired by the ACK theory [3]. However, different hypotheses were used in the present work, which are more appropriate to our problem where various specimen geometries are considered. Characterization of fibre failure, ε_{a2}, involved a numerical simulation of the fibre failure process. A distribution of failure stresses was assumed for individual fibres, which was empirically related to the ultimate strain, ε_{a2}.

It was assumed that matrix cracking was determined by a decrease of the total energy, in such a way that a minimum in the elastic energy, W_e, was reached. The conditions were

$$W_{ex} > W_e + W_f \tag{9}$$

$$dW_e/dl_a = 0 \tag{10}$$

where W_{ex} is the external work. W_e and W_f were derived from Equations 5 and 6. We assumed that the strain remained constant during cracking, and that the external work was consequently nil. This hypothesis was chosen with the purpose of keeping the elementary cells independent, because matrix cracking in one cell did not induce any change in the neighbouring ones. The derivation of ε_{a1} and l_a from Conditions 9 and 10 is described in [8]. The calculation is tedious but presents no difficulty. Therefore only the final result is given here. It appeared that the length l_a, was close to the transfer distance l_c, of stress along the interface [3].

$$l_a = \lambda l_c = \lambda \frac{r_f}{2} \frac{E_m V_m \sigma_a}{E_c V_f \tau_i} \tag{11}$$

λ depends on the parameter E_f'/E_c, and it always falls between 0.95 and 1. Assuming $l_a = l_c$, the critical strain, ε_{a1}, is given by:

$$\varepsilon_{a1} = \left[\frac{12\gamma_m E_f V_f^2 \tau_i}{E_c E_m^2 V_m r_f}\right]^{1/3} \frac{E_c + E_f'}{2E_f'} \left[\frac{4E_f'}{3E_c + E_f'}\right]^{1/3} \tag{12}$$

It should be noted that this analysis presents two differences from the ACK theory: Averston *et al.* [3] assumed that the distance l_a was identical to the report distance, l_c, and that the load remained constant during cracking. The external work was thus different from zero, and the critical strain was lower than the

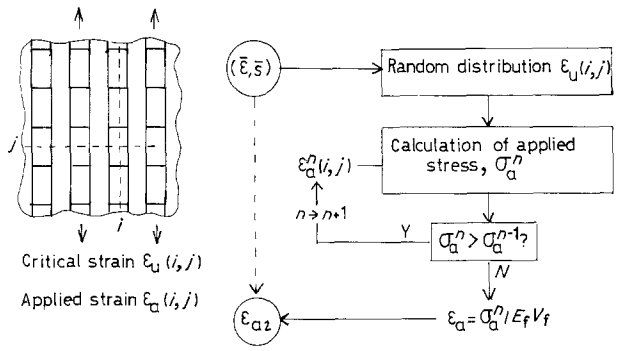

Figure 9 Numerical simulation of the fibre failure process. The critical strain, ε_{a2}, is computed from a random distribution of critical strain following a Gaussian distribution (average value $\bar{\varepsilon}$ and standard deviation $\bar{s}$).

value predicted by Equation 12. The strains obtained using both approaches are compared in Fig. 8.

The relation between the ultimate strain of the composite, ε_{a2}, and the failure strain of fibres, ε_{fu}, was derived from data generated by a numerical simulation of the fibre failure process (Fig. 9). Each fibre was shared in elementary cells characterized by their own failure strain. Bundles were described as bidirectional networks of elementary cells (Fig. 9). The failure strain of this network was predicted from assumed failure strain distributions for individual cells. For this purpose, Gaussian distributions were numerically generated, for various values of average strain, $\bar{\varepsilon}$, and standard deviations, $\bar{s}$. As previously, the applied strain distributions induced by loading conditions were similar to those existing in continuous materials: uniform in tensile specimens and varying linearly in bending specimens. The simulation was carried out step by step, at increasing values of the applied strain. At each step, the cells which experienced fracture were determined. It was assumed that failure of one cell caused failure of the fibre. Because the matrix was already cracked, no transfer of strain from a broken fibre to the neighbouring fibres was considered. The average applied stress was then obtained from the local stresses endured by the surviving fibres.

Variations of the average stress with the applied strain showed that the stress reached a maximum for fractions of broken fibres of about 15%. Beyond this level, the stress decreased rapidly. These variations are similar to the unstable failure process depicted in Fig. 6. Based upon energy considerations, one may consider that unstable fracture of the remaining fibres occurs near the maximum of the average stress. This is also due to the elasticity of the fixture. Ultimate fracture of the composite was assumed to occur at this stress level.

Determination of ε_{a2} as a function of fibre properties required iterative computations for various couples ($\bar{\varepsilon}$, $\bar{s}$). For each couple, the strains obtained from numerous computations were expressed in terms of an average value, ε_a, and standard deviation, s_a. Different pairs of data (ε_a, s_a) were predicted for one fibre and a larger quantity of fibres, in tensile and bending conditions. Variations of the input parameters ($\bar{\varepsilon}$, $\bar{s}$) revealed that the following linear equations were satisfied

$$\varepsilon_a = \bar{\varepsilon} - t_\varepsilon \bar{s} \quad (13)$$

$$s_a = t_s \bar{s} \quad (14)$$

where t_ε and t_s are constant in a given configuration. Empirical values of parameters t_ε and t_s are given in Table II for the four configurations. The relation between the ultimate strain of the composite (ε_{a2}, s_2) and that of individual fibres in tensile conditions (ε_{fu}, s_f) was obtained by comparing the results of computations for one fibre and for a large quantity of fibres (more than 10). The following relations were obtained

TABLE II Empirical values of parameters t_ε and t_s, obtained using a large number of computations. These parameters are constant for quantities of fibres larger than about 10

	Tensile tests		Bending tests	
	1 fibre	$N > 10$ fibres	1 fibre	$N > 10$ fibres
t_ε	2.4 ± 0.2	2.8 ± 0.2	1.2 ± 0.5	1.6 ± 0.3
t_s	0.4	0.2	0.5	0.3

tensile:

$$\varepsilon_{a2} = \varepsilon_{fu} - s_f \quad (15)$$

$$s_2 = 0.5\, s_f \quad (16)$$

bending:

$$\varepsilon_{a2} = \varepsilon_{fu} + 2s_f \quad (17)$$

$$s_2 = 0.75\, s_f \quad (18)$$

3. Application: prediction of the mechanical behaviour of the C/SiC and SiC/SiC composites

The constitutive laws relevant to the considered composites were determined from the experimental stress–elastic strain curves recorded on tensile tests. Relations between these curves and the parameters describing the constitutive law are shown in Fig. 10. The values of E_c, E_f', ε_0, ε_{a1} and ε_{a2} were obtained by fitting the theoretical stress–elastic strain relation to experimental data, as shown in Fig. 11. The parameters of the constitutive law are summarized in Table III. The parameter $\gamma_m V_m / l_a$ was estimated from

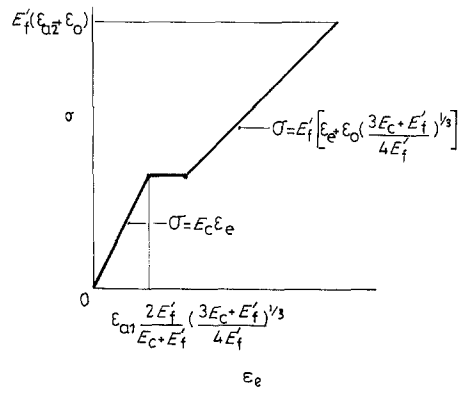

Figure 10 Theoretical stress–elastic strain curve for a tensile test with compliant test fixture.

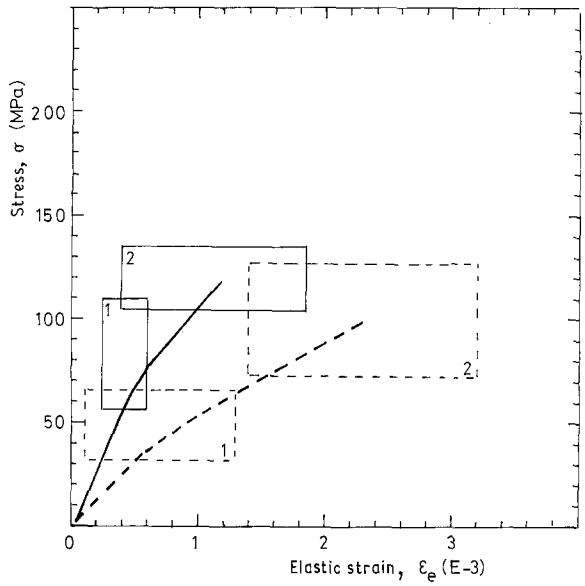

Figure 11 Fitting of theoretical stress–elastic strain relations to the experimental data measured on tensile tests. Experimental data are given by areas 1 and 2, corresponding to matrix cracking and fibre failure, respectively. Each side represents the average value ± standard deviation. (– – –) C/SiC, (——) SiC/SiC.

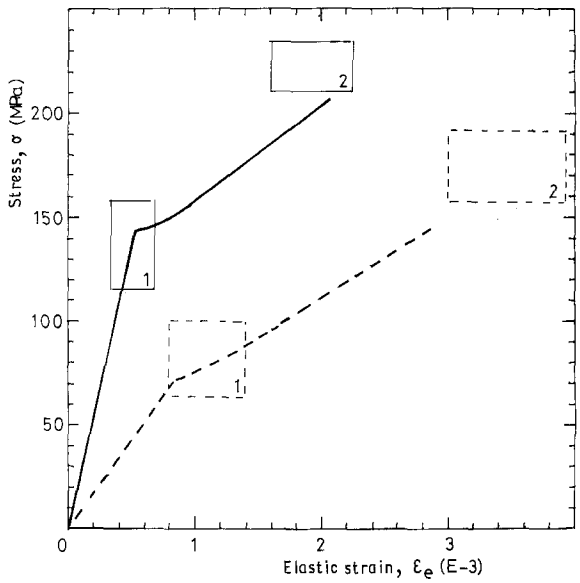

Figure 12 Comparison of theoretical stress–elastic strain curves with experimental data for the bending specimens. The theoretical results were calculated from data of Table III. Experimental data are represented by areas 1 (matrix cracking) and 2 (fibre failure). Each side represents the average value ± standard deviation. (– – –) C/SiC, (——) SiC/SiC.

the average distance, l_a, measured on fractured specimens (50 μm in C/SiC and 20 μm in SiC/SiC [1]), and for a surface energy $\gamma_m = 25\ J\ m^{-2}$ (average of the surface energies usually measured in monolithic silicon carbide). The shear strength at the fibre/matrix interface was derived from the values of l_a and ε_{a1}, using Equations 11 and 12.

The stress–elastic strain curves predicted for the bending specimens are shown in Fig. 12. The simulation method of Section 2.2 was applied first using data of Table III. As already observed from Fig. 7, matrix cracking and non-linear behaviour are characterized by stress levels higher than previously found with tensile tests (Fig. 11), whereas ultimate fracture occurred at the same level of elastic strain in both loading geometries

$$(\varepsilon_e)_u = \varepsilon_{a2} - \varepsilon_0\left[\left(\frac{3E_c + E'_f}{4E'_f}\right)^{1/3} - 1\right] \quad (19)$$

This strain level was refined, using the results of fracture process simulation described in Section 2.3. The tensile strain, ε_{a2}, given by Equations 15 to 18, was incorporated into Equation 19. Using the standard deviations, s_f, derived from experimental data obtained in tensile tests (values of parameter s_2 reported in Fig. 11) this led to predictions which were not consistent with experimental data: the tensile strains were thus higher than expected when compared with the bending results. Considering that these standard deviations might involve an additional discrepancy induced by the test procedure, s_f values were then estimated from the experimental data obtained on bending tests (0.08% and 0.04%, respectively, were obtained for C/SiC and SiC/SiC). It can be seen from Fig. 12 that predictions are now in agreement with experimental data as shown by the consistency of the predicted linearity limit and ultimate failure with experimental values of $(\varepsilon_{a1}, \sigma_1)$ and $(\varepsilon_{a2}, \sigma_2)$. This agreement is, however, weakened by the significant scatter exhibited by experimental data. Besides the use of a simplified approach to stress and strain calculations, the contribution of other factors related to the material itself may also be invoked to explain differences observed in tensile and bending tests. The present results show that this contribution should be limited, and should have the same magnitude as the data scatter.

TABLE III Experimental values obtained for the constitutive law parameters

Parameter	C/SiC	SiC/SiC
E'_f (GPa)	32	48
E_c (GPa)	85	215
ε_0 (10^{-3})	0.4	0.4
ε_{a1} (10^{-3})	0.8	0.7
ε_{a2} tensile (10^{-3})	2.8	2.1
$\gamma_m V_m/l_a$ $(MJ\ m^{-3})$	0.3	0.6
l_a (μm)	50	25
τ_i (MPa)	5	20
ε_{a2} bending (10^{-3})	5.2	3.3

The predictions of residual strain, ε_r, and absorbed energy, W_f, are plotted on Fig. 13. An average slope, P_ε, of about 0.2 was obtained for the residual strain–elastic strain plots in both materials. This parameter involves only the residual strain related to the stress mismatch existing between fibres and cracked matrix. Calculation of the absorbed energy showed that the term related to the surface energy is preponderant in both composites. This result is partly due to low interfacial shear strength, which results in a negligible frictional term. The plot of absorbed energy against elastic strain is linear in bending tests only. In tensile tests, the theoretical slope, P_w, was therefore estimated from the ultimate values (it should be noted

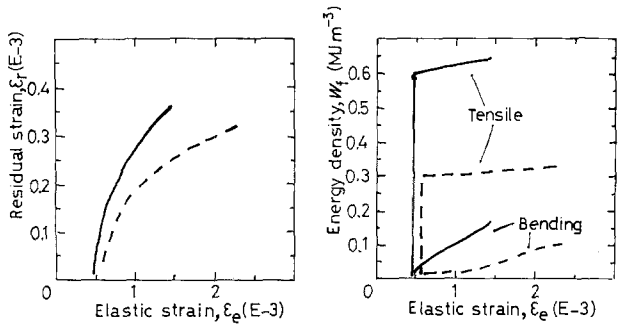

Figure 13 Prediction of residual strain, ε_r, and absorbed energy, W_f, for (– – –) C/SiC and (——) SiC/SiC.

TABLE IV Values of the parameters describing the residual behaviour

Parameter	C/SiC		SiC/SiC	
	Experiment	Theory	Experiment	Theory
$P_\varepsilon = \dfrac{\Delta\varepsilon_r}{\Delta\varepsilon_e}$	3.0 ± 1.3	0.2	0.4 ± 0.3	0.2
$P_w = \dfrac{\Delta W_f}{\Delta\varepsilon_e}$ (MJ m^{-3})				
Tensile	141 ± 51	57	50 ± 32	125
Bending	22 ± 6	12	5 ± 0.5	25

that the ratio between the values of P_w predicted in tensile and bending tests is consistent with those estimated in Part 1 [1]). The experimental and calculated results* (Table IV) exhibit a certain discrepancy which may be attributed to damage in the bundles framework. In the SiC/SiC material, the contribution of the framework is limited, and is hindered by the scatter in experimental data. The theoretical value of the energy, which is larger than the experimental ones, may be considered to be overestimated. Assuming that the value of the surface energy is correct, this overestimation may be related to an incomplete matrix cracking, leading to a process zone smaller than that predicted by the model, and consequently to a lower amount of energy per unit volume. In the C/SiC composite, the main part of the residual strain seems to affect the bundle framework. The absorbed energy is also larger than the theoretical contribution of the bundles. However, owing to data scatter and a possible overestimation, as previously observed with SiC/SiC, the energy dissipated in the framework could not be predicted accurately.

4. Discussion: prediction of the mechanical behaviour from fibre and matrix properties

The results reasonably allow one to consider that the constitutive law described by the data of Table III is representative of the composite's behaviour. It is now interesting to compare these data with those calculated from fibre and matrix properties. The data related to the elastic modulus were discussed in Part 1 [1]. Data pertinent to matrix cracking and fibre failure are discussed below.

4.1. Matrix cracking

The critical strains at matrix cracking were estimated from Equation 12, using constituent properties available in the literature (Table I, Part 1 [1]). Strains of 0.20% and 0.29% were predicted, respectively, for the C/SiC and SiC/SiC composites (265 and 365 MPa for the respective critical stresses). These data are much higher than the experimental ones (0.08% and 0.07%, respectively, in Table III). A comparable discrepancy was obtained with the ACK theory, because predictions of 0.12% and 0.23% must be compared to experimental elastic strains† of 0.05% and 0.06% for C/SiC and SiC/SiC, respectively. These discrepancies may be attributed to various factors, as discussed thereafter.

The accuracy of Equation 12 used to calculate the critical strain is first involved. The confidence level in predictions mainly depends on the strain distribution considered for the composite having a cracked matrix, and on the accuracy in constituent properties. The approximate strain distribution given by Equation 8 was found to be consistent with numerical computations of the strain field in a system consisting of a fibre surrounded by a cracked matrix [8]. Only a poor estimation of the fibre, matrix and interface properties is possible due to the lack of experimental data. However, Equation 12 shows that a given uncertainty in the constituent properties will induce a smaller one in the critical strain. For example, a ten-fold overestimation of the interfacial shear strength (which is highly improbable) will only result in a critical strain of double the value. Misestimations may also be counterbalanced by an error in another parameter.

The presence of residual thermal strains in the composites can affect the critical strain of the matrix. Residual strains are common in composite materials and can be estimated approximately [9, 10]. In the C/SiC material, high tensile residual strains are expected in the matrix. Assuming a processing temperature of 1000 °C, realistic thermal stresses of about 500 MPa were predicted based on the thermal expansion coefficients pertinent to fibres and matrix [10]. However, these stresses are likely to be released through displacements occurring at the interfaces, because a low interfacial shear strength of 5 MPa was estimated for the C/SiC. Evaluation of thermal stresses is then not straightforward. However, they cannot be discounted. In the SiC/SiC material, the thermal expansion coefficients of the fibre and of the matrix are very similar. Therefore, the thermal stresses are negligible.

Microstructural defects and matrix porosity are probably the main origins of the low critical strains

* P_w values were divided by 2 to take into account the bidirectional structure of the materials.
† The critical strain in the ACK theory corresponds to the start of non-linearity (Figs 10 and 11).

which have been observed. Unfortunately, estimation usually involves numerical techniques. Solutions are available only for particular configurations [11, 12]. However, results show that when the fibres are less stiff than the matrix, the conditions for crack growth from a matrix flaw are similar in composites and in monolithic materials. In the C/SiC and SiC/SiC composites, cracks are likely to initiate at the large pores located in the matrix. The critical strain then depends mostly on the local stresses operating on these flaws.

4.2. Fibre failure

Fracture strains of individual fibres within the composite were estimated from ε_{a2} values using Equations 15 to 18. Using the values of s_f estimated in Section 3, ultimate strains, ε_{fu}, of 0.36% and 0.25% were predicted for the carbon and SiC fibres, respectively (which corresponds to failure stresses of 650 ± 150 MPa for the carbon fibres and 480 ± 80 MPa for the SiC ones). The fibre strength data available in the literature are usually measured on individual fibres using tensile tests. For gauge lengths of 10 to 20 mm (similar to those used in the present work), strengths of about 3 and 1.5 GPa are reported for commercial carbon and silicon carbide fibres [13, 14]. However, the carbon fibres incorporated in the C/SiC composites under consideration contain more impurities than the commercial ones, and are expected to exhibit a strength value lower by about one-half. In the SiC/SiC composite, an alteration of the fibre properties during manufacture of the composite is likely to occur. A decrease in the strength of silicon carbide fibres was reported above a temperature of 800 °C [14]. At 1000 °C, the decrease in the strength is about 300 MPa. Therefore, it may be reasonably considered that the strengths of the carbon and SiC fibres should be about 1500 and 1200 MPa, respectively, which is still about twice as high as the predictions. The difference between the failure of single fibres, tested individually or considered within the composite may be attributed to an effect of the matrix, which affects fibre loading conditions: the cracked matrix thus induces a non-uniform strain distribution [3], and a multiaxial stress state may exist, due to irregularities in the fibre network.

The effect of non-uniform strains was approached as follows: with a non-uniform strain distribution, approximately described by Equation 7 the criticality of the fibre flaws depends on their location within the fibres. Defects with remote location with respect to the matrix cracks are expected to be less critical than those lying in the crack planes.

This phenomenon induces significant changes in the strength distribution of the fibres incorporated in the composite. These changes were estimated assuming a simple Weibull strength distribution.

$$p = 1 - \exp - V_e(\sigma/\sigma_0)^m \qquad (20)$$

where p is the probability of rupture under a stress σ, and m and σ_0 are the Weibull parameters. In a tensile test, the effective volume V_e represents the volume of the fibre. For a fibre surrounded by matrix, the effective volume was calculated from a strain distribution obtained by a numerical method [8]. An approximate value is given by

$$V_e = \pi r_f^2 l\lambda = \pi r_f^2 l\left\{\frac{r_f}{2l_a}\frac{1}{m+1}\frac{\sigma_a}{\tau_i}\left[1-\left(1-\frac{2l_a}{r_f}\frac{\tau_i}{\sigma_a}\right)^{m+1}\right]\right\} \qquad (21)$$

This relation is close to those obtained by other authors using different strain distributions [15]. The effective volume calculated from Equation 21 is smaller than the volume of fibres ($\lambda < 1$), showing that the stresses operating on fibres at failure must be higher when fibres are incorporated in the composite than when they are isolated. Applied to the C/SiC and SiC/SiC composites, Equation 21 gave respective values of 0.6 and 0.8 for λ, leading to stress increases of 200 and 100 MPa, respectively, in the C/SiC and the SiC/SiC composites. This matrix effect then enhances the discrepancy observed between fibre properties and predictions.

Polyaxial stress states are likely to appear during damage of the composites. In particular, geometrical irregularities in the fibre network and residual displacements in the matrix or at fibre/matrix interfaces are likely to induce locally shear forces or bending momentum in the fibres. These additional forces have an unpredictable location and they are therefore difficult to calculate. Nevertheless, on the basis of the differences between theoretical and experimental data, one may draw the conclusion that the polyaxial loading of fibres induces additional stresses having a magnitude comparable to the initial uniaxial tensile stress. Despite the lack of accuracy on predictions, this assumption seems to be reasonable.

5. Conclusion

A model for the mechanical behaviour of the two bidirectional woven C/SiC and SiC/SiC composites was proposed. The model was based on a constitutive law considering the typical damaging process observed in these materials, assuming defect-free fibres and matrix. This constitutive law was used to predict the macroscopic behaviour of tensile and bending loading geometries. By comparing the experimental results with predictions based on fibre and matrix properties, the model also allowed estimation of the contribution of the woven structure to the damage and the effect of the microstructural defects on the mechanical behaviour.

The discrepancies observed between the results of tensile and bending tests were satisfactorily explained by the model. In particular, the higher modulus of rupture measured in bending was related to the effect of non-linear behaviour on stress calculation, and to the effect of specimen geometry on the fibre failure process. The damage was described in terms of residual strain and energy absorbed in the whole specimen. Consistent results were obtained for both geometries, with similar residual strains and an absorbed energy related to the strain distribution in the speci-

men. However, the accuracy of results was limited by the scatter in experimental data.

The critical strains characterizing matrix cracking and fibre failure, were found to be much lower than those predicted from fibre and matrix properties. Despite the lack of data on the properties of the constituents, the difference seemed mainly to be due to the geometrical irregularities of reinforcement and to matrix flaws. By inducing premature damage in the materials, they prevent the fibres from fulfilling the optimum possibilities of reinforcement. The theoretical constitutive law thus represents the optimum behaviour that could be expected for a given combination of constituents, rather than the real behaviour. It can, however, provide a useful guideline for selecting appropriate fibre/matrix couples and for improving the existing composites.

Acknowledgement

This work was supported by DRET under contracts no. 82 305 and 84 082.

References

1. E. INGHELS and J. LAMON, *J. Mater. Sci.* **26** (1991) 540.
2. D. B. MARSHALL and A. G. EVANS, *J. Amer. Ceram. Soc.* **68** (1985) 225.
3. J. AVESTON, G. A. COOPER and A. KELLY, "Single and Multiple Fracture", in "Properties of Fiber Composites" (IPC Science and Technology Press, Guilford, Surrey, 1971) pp. 15–24.
4. V. LAWS, *J. Mater. Sci.* **16** (1981) 1299.
5. G. BERNHART, "Relations entre les résultats d'essais de flexion et d'essais de traction pour des composites à matrice rigide", in Proceedings JNC4 (September 1984, Editions Pluralis, Paris) pp. 75–92.
6. D. G. HARLOW and S. L. PHOENIX, *Int. J. Fract.* **15** (1979) 321.
7. K. P. OH, *J. Compos. Mater.* **13** (1979) 311.
8. E. INGHELS, PhD thesis, Ecole Nationale Supérieure des Mines de Paris, Paris, June 1987.
9. I. W. DONALD and P. W. McMILLAN, *J. Mater. Sci.* **11** (1976) 949.
10. D. C. PHILLIPS, "Fibre Reinforced Ceramics", Report AERE-R10056, Harwell, Oxfordshire, February 1981.
11. G. C. SIH, *Mech. Fract.* **6** (1981).
12. MING-CHE LU and F. ERDOGAN, *Engng Fract. Mech.* **18** (1983) 491.
13. J. L. G. SILVA and D. J. JOHNSON, *J. Mater. Sci.* **19** (1984) 3201.
14. G. SIMON and A. R. BÜNSELL, *ibid.* **19** (1984) 3649.
15. A. G. EVANS, *Mater. Sci. Engng* **71** (1985) 3.

Received 24 November
and accepted 1 December 1989